Versatile and competing spin-charge-orbital orders in the bilayered manganite system $Pr(Sr_{1-y}Ca_y)_2Mn_2O_7$

Y. Tokunaga,[1,2] T. J. Sato,[3] M. Uchida,[2] R. Kumai,[4] Y. Matsui,[5] T. Arima,[2,6] and Y. Tokura[1,2,4,7]

[1]*Multiferroics Project, ERATO, Japan Science and Technology Agency (JST), Bunkyo-ku, Tokyo 113-8656, Japan*

[2]*Spin Superstructure Project, ERATO, JST, Tsukuba, Ibaraki 305-8562, Japan*

[3]*Neutron Science Laboratory, Institute for Solid State Physics, University of Tokyo, 106-1 Shirakata, Tokai, Ibaraki 319-1106, Japan*

[4]*Correlated Electron Research Center (CERC), National Institute of Advanced Industrial Science and Technology (AIST), Tsukuba, Ibaraki 305-8562, Japan*

[5]*Advanced Materials Laboratory, National Institute for Materials Science (NIMS), Tsukuba 305-0044, Japan*

[6]*Institute of Multidisciplinary Research for Advanced Materials, Tohoku University, Sendai 980-8577, Japan*

[7]*Department of Applied Physics, University of Tokyo, Bunkyo-ku, Tokyo 113-8656, Japan*

(Received 15 December 2007; revised manuscript received 25 December 2007; published 25 February 2008)

Electronic-phase competition has been investigated for single crystals of half-doped bilayer-structure manganites, $Pr(Sr_{1-y}Ca_y)_2Mn_2O_7$ ($0 \leqslant y \leqslant 1.0$), with controlled one-electron bandwidth (W). For $y \leqslant 0.4$, the A-type antiferromagnetic (AF) state with x^2-y^2 orbital order shows up as the ground state while accompanying the short-range vertical charge order with the periodicity of $\approx 4a_0$ ($a_0 \approx 0.4$ nm). For $y > 0.4$, with reduced W, the CE-type AF state emerges with the ordered staggered orbitals ($3x^2-r^2/3y^2-r^2$) whose diagonal stripes undergo the 90° rotation with decreasing temperature, perhaps coupled with the evolution of spin correlation.

DOI: 10.1103/PhysRevB.77.064428 PACS number(s): 75.30.Kz, 71.30.+h

Spin, charge, and orbital degrees of freedom for strongly correlated d electrons in a solid form versatile electronic phases which occasionally compete with each other and give rise to the bicritical or multicritical states with respect to one or more control parameter(s). One of the most typical examples is the hole-doped perovskite manganites showing the colossal magnetoresistance (CMR).[1] In the nearly half-doped manganites, the ferromagnetic metallic (FM) state competes with various other orbital-charge-spin ordered phases, typically the CE-type antiferromagnetic charge-ordered and orbital-ordered (CO-OO) insulating state [see Fig. 2(a), inset]. Another competing phase may be the A-type (layered-type) antiferromagnetic (A-AF) pseudometallic state with x^2-y^2 orbital order [see Fig. 1(a), inset], viewed as the two-dimensional (2D) analog of the double-exchange (DE) mediated FM state. The critical competition among these phases is tuned by control parameters, such as the one-electron bandwidth W (electron hopping interaction) and the band filling (hole-doping level), as well as external perturbations, e.g., magnetic field and other stimulations.[1] In this context, another important control parameter is the electronic dimensionality, as realized by the layered-perovskite or Ruddlesden-Popper series crystal structure. In single-layered (K_2NiF_4 type) manganites $La_{1-x}Sr_{1+x}MnO_4$, for example, there appears no more DE mediated FM nor A-AF state because of too much reduction of the transfer interaction, while the CE-type CO-OO state dominates the electronic-phase diagram in the moderately ($x \sim 0.5$) or heavily ($x \geqslant 0.5$) hole-doped state.[2] In the bilayered compounds $La_{2-2x}Sr_{1+2x}Mn_2O_7$, on the other hand, the FM, A-AF, and CE-type CO-OO states can be all seen similarly to the pseudocubic (infinite-layer) perovskite manganites, although the relative stability of the three-dimensional FM state is much reduced.[3,4] Furthermore, such a moderate reduction of the electronic dimensionality as in the bilayered structure is anticipated to bring about the interesting phenomena arising from the phase instability, such as the nesting of the quasi-2D Fermi surface[5,6] or the emergence of the ferroelectricity in the CO-OO state.[7] In the case of the bilayered manganites with composition of $R_{2-2x}Sr_{1+2x}Mn_2O_7$ (R being a small rare-earth ion and $x \sim 0.5$), however, the reduced electronic dimension appears to make the system more amenable to the quenched disorder arising from the mismatch of the ionic sizes of R^{3+} and Sr^{2+},[8] stabilizing the spin-glass state[9] apart from the long-range A-AF state for R=La, Pr, and Nd.[10,11] To unambiguously pursue the bicritical phase competition in the reduced dimension for the CMR manganites, we have examined here the electronic phases with variation of W for the bilayered manganites, while keeping the effect of the quenched disorder minimal, by employing the single crystals of $Pr(Sr_{1-y}Ca_y)_2Mn_2O_7$ (x=0.5, $0 \leqslant y \leqslant 1.0$), which is the 2D analog of the similar minimal-disorder system of perovskite $Pr_{1-x}Ca_xMnO_3$ ($x \sim 0.5$) with the minimal mismatch of the ionic size of Pr^{3+} and Ca^{2+}.[1] The major phase competition is observed to occur between the CE-type CO-OO and the A-AF states, while accompanying rich interesting features such as the polar and/or nonpolar CO-OO state and the vertical charge stripes in the A-AF state.

Single crystals of $Pr(Sr_{1-y}Ca_y)_2Mn_2O_7$ ($0 \leqslant y \leqslant 1.0$) were melt grown by a floating zone method with a typical feed speed of 8–12 mm/h in the atmosphere of 1–8 atm oxygen. Averaged structures are changed from tetragonal $I4/mmm$ for $PrSr_2Mn_2O_7$ ($a=b=3.8535$ Å and $c=19.928$ Å at 300 K) to orthorhombic $Amam$ ($a=5.4060$ Å, $b=5.4671$ Å, and $c=19.221$ Å at 290 K) for $PrCa_2Mn_2O_7$ which has tilts of MnO_6 octahedra around the a axis. Such an orthorhombic distortion as resulting from a small average radius of the A-site cations except for the Ca-poor ($y < 0.2$) crystals enabled us to control W via change of Mn–O–Mn bond angles, similar to the pseudocubic perovskite case.[1] The Ca-rich crystals are orthorhombically distorted and hence contain fine ab twin domains (bandlike shape with a typical width of

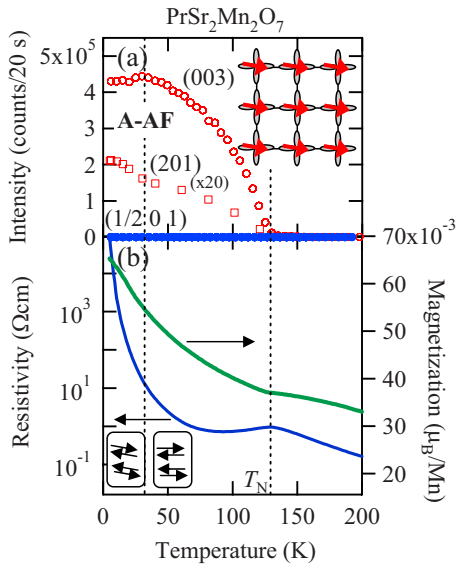

FIG. 1. (Color online) Temperature dependence of (a) peak intensities of magnetic Bragg reflections at selected positions, (b) M_{ab} in the magnetic field of $\mu_0 H=0.5$ T, and ρ_{ab} for $PrSr_2Mn_2O_7$ (A-AF). The inset figure of (a) shows the schematic of the orbital and the spin arrangement in the MnO_2 plane for A-AF and the inset figures of (b) indicate the schematic of the stacking pattern of manganese moments along the c axis.

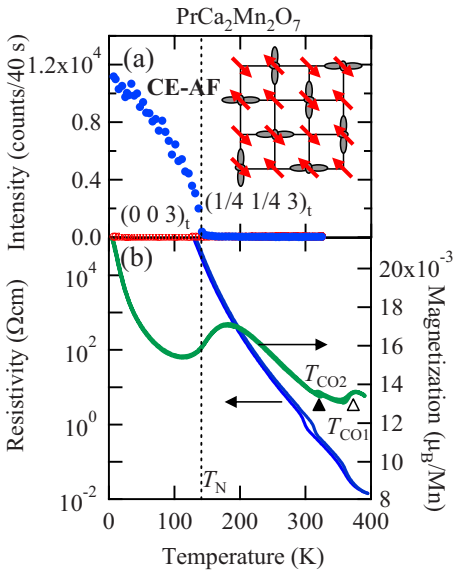

FIG. 2. (Color online) Temperature dependence of (a) peak intensities of magnetic Bragg reflections at selected positions, (b) M_{ab} in the magnetic field of $\mu_0 H=0.5$ T, and ρ_{ab} for $PrCa_2Mn_2O_7$ (CE-AF). The inset figure of (a) shows the schematic of the orbital and the spin arrangement in the MnO_2 plane for CE-AF.

tens of microns). Resistivity in the ab plane (ρ_{ab}) was measured by a conventional four-probe method. In-plane components of magnetization (M_{ab}) were measured by a commercial superconducting quantum interference device magnetometer. Single-crystal neutron scattering measurements were carried out with the triple-axis spectrometer GPTAS installed at JRR-3, Tokai, Japan. The measurements were done on the $(h0l)$ reciprocal zone for $PrSr_2Mn_2O_7$ and the pseudotetragonal $(hhl)_t$ reciprocal zone for $PrCa_2Mn_2O_7$. Single-crystal x-ray diffraction measurements were done in $PrSr_2Mn_2O_7$ with the use of synchrotron radiation (SR) x ray and a four-circle diffractometer at the beamline 4C at the Photon Factory, High Energy Accelerator Research Organization (KEK), Japan. Electron diffraction patterns (EDPs) and dark field images (DFIs) were collected by transmission electron microscopes (TEMs) (Hitachi HF-3000L and Hitachi HF-3000S TEM) operated at 200 kV. For the TEM measurement, the thin specimens of the $PrCa_2Mn_2O_7$ crystal were prepared by Ar^+ ion milling.

Figure 1(a) shows the temperature dependence of magnetic Bragg intensity at selected positions and Fig. 1(b) shows M_{ab} and ρ_{ab} for $PrSr_2Mn_2O_7$. With decreasing temperature, the peak intensity at $\boldsymbol{Q}=(0, 0, 3)$ and $(2, 0, 1)$, a measure of the order parameter of A-AF, increases monotonically below $T_N=130$ K except for $T<30$ K, while the $\boldsymbol{Q}=\left(\frac{1}{2},0,1\right)$ peak (characteristic of CE-AF) is not discerned in any temperature range. The subtle reduction of $(0, 0, 3)$ intensity and increase of $(2, 0, 1)$ intensity below 30 K indicate the slight canting of magnetic moments of Mn ions toward the out-of-plane direction. A similar reorientation behavior is also reported for $NdSr_2Mn_2O_7$.[10,11] T_N is coincident with the temperature where M_{ab} shows an inflection and ρ_{ab} starts to decrease. The metalliclike behavior right below T_N is consistent with the magnetic structure of A-AF with x^2-y^2-type OO, as observed for the pseudocubic manganite with A-AF,[12] but the low-temperature divergence of ρ_{ab} indicates the strong charge localization, whose origin will be discussed later. On the other hand, the monotonic increase of the peak intensity at $\boldsymbol{Q}=\left(\frac{1}{4},\frac{1}{4},3\right)_t$ (characteristic of CE-AF) with decreasing temperature is observed for $PrCa_2Mn_2O_7$ from the temperature at which M_{ab} shows an inflection [$T_N \sim 143$ K, see Figs. 2(a) and 2(b)], while the peak at $\boldsymbol{Q}=(0, 0, 3)_t$ is not found. No anomaly is observed for ρ_{ab} at around T_N. These results indicate that the magnetic structure of $PrCa_2Mn_2O_7$ is CE-AF below T_N down to the lowest temperature. Figure 3 shows the temperature dependence of ρ_{ab} and M_{ab} for $Pr(Sr_{1-y}Ca_y)_2Mn_2O_7$. For $y<0.4$, a quasimetallic behavior is observed right below T_N, suggesting that the magnetic structure is A type. For $y>0.4$, the abrupt suppression of magnetization and the steep increase of ρ_{ab} are observed simultaneously with the decrease of temperature, signaling the CO-OO transition. The ρ_{ab} of the $y=0.4$ compound shows both a steep upturn below $\sim$180 K and a metalliclike behavior below $\sim$110 K, i.e., the coexistence of the A- and CE-AF phases. Note that for a high-y region, the CO transition clearly splits into T_{CO1} and T_{CO2}. Both of the CO transition temperatures increase with y. For $y=1$, T_{CO1} and T_{CO_2} reach $\sim$375 and $\sim$323 K, respectively.

We summarize in Fig. 4 the phase diagram obtained by the magnetization and resistivity measurements. The boundary between the competing two phases, A-AF pseudometallic (A-AFM) and CE-AF insulator (CE-AFI), is around $y\sim0.4$. Toward $y\sim0.4$, the two CO-OO transition temperatures steeply decrease, while T_N is rather flat against y. This suggests that the CO-OO transition is more stabilized by a larger

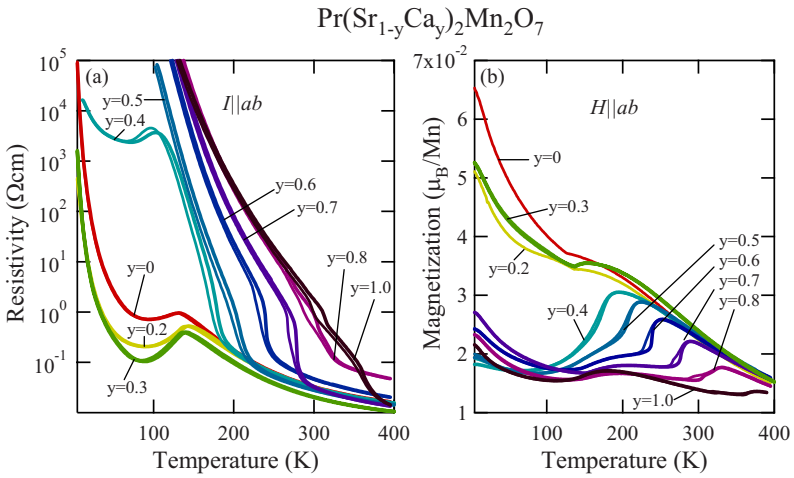

FIG. 3. (Color online) Temperature dependence of (a) ρ_{ab} and (b) M_{ab} for $Pr(Sr_{1-y}Ca_y)_2Mn_2O_7$ ($y=0-1.0$). M_{ab} was measured under a magnetic field of $\mu_0 H=0.5$ T.

orthorhombic distortion or a narrowed W, while the spin order is affected also by the change of W. The A-AF spin arrangement with x^2-y^2-type OO is realized for $y=0$ with relatively wide W. In this state, e_g electrons are more or less delocalized on the MnO_2 plane (composed of FM 2D sheet) due to the DE mechanism. On the other hand, for $y=1$, charges are strongly localized in the FM quasi-one-dimensional (1D) zigzag chains composed of $3x^2-r^2/3y^2-r^2$ staggered-type orbital arrangement. Such reduction of the electronic dimensionality (from 2D to quasi-1D) is obviously the consequence of the reduction of the W or the DE interaction. The clear-cut bicritical nature of the phase diagram may result from the relatively small randomness of the system.[1,13–15]

The phenomenon of rotation of orbital stripes as reported previously for the $y=0.9$ compound[7] was confirmed to be present in the present system over a wide range of y ($y \geqslant 0.5$). Figures 5(a) and 5(b) show the [001] zone-axis EDP of $PrCa_2Mn_2O_7$ crystal at 340 and 290 K, respectively. Below T_{CO1}, satellite spots appear at around each fundamental reflection. The modulation vector is described as $\boldsymbol{q}=\pm\boldsymbol{b}^*/2(b^*=2\pi/b)$; the orbital stripe is running along the a axis, as depicted in Fig. 5(c). Below T_{CO2}, however, the satellite spots along the b^* axis disappear and those with

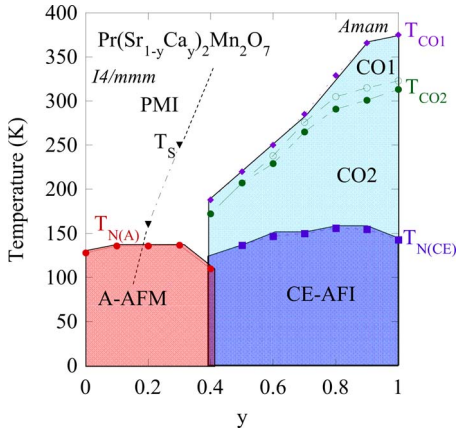

FIG. 4. (Color online) Electronic phase diagram of $Pr(Sr_{1-y}Ca_y)_2Mn_2O_7$ ($y=0-1.0$). T_{CO1} and T_{CO2} with thermal hystereses and T_N of A-AF ($T_{N(A)}$) and CE-AF ($T_{N(CE)}$) are determined from resistivity and magnetization measurements. T_S represents the structural transition from tetragonal to orthorhombic (see main text). Dashed lines are a guide to the eyes.

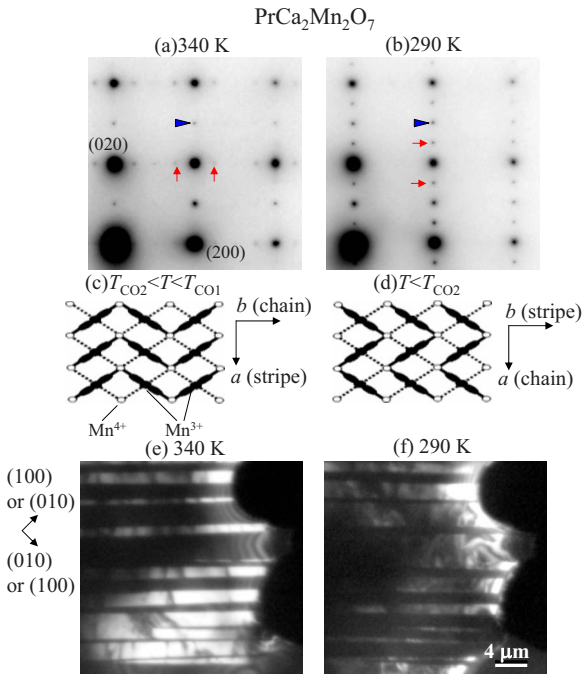

FIG. 5. (Color online) [(a) and (b)] EDPs of the [001] zone for $PrCa_2Mn_2O_7$ taken at (a) 340 K and (b) 290 K. The triangle indicates the spot arising from the A-centered orthorhombic structure. The vertical arrows indicate superlattice spots. [(c) and (d)] Schematics of CO-OO patterns for (c) $T_{CO2} \leqslant T \leqslant T_{CO1}$ and (d) $T \leqslant T_{CO2}$ in the MnO_2 plane, respectively. [(e) and (f)] DFIs taken with the aperture fixed at the position of the one CO-OO reflection position of the CO1 phase at (e) 340 K and (f) 290 K. Bright and dark contrasts correspond to structural twins in which the orbital stripe directions are different by 90°.

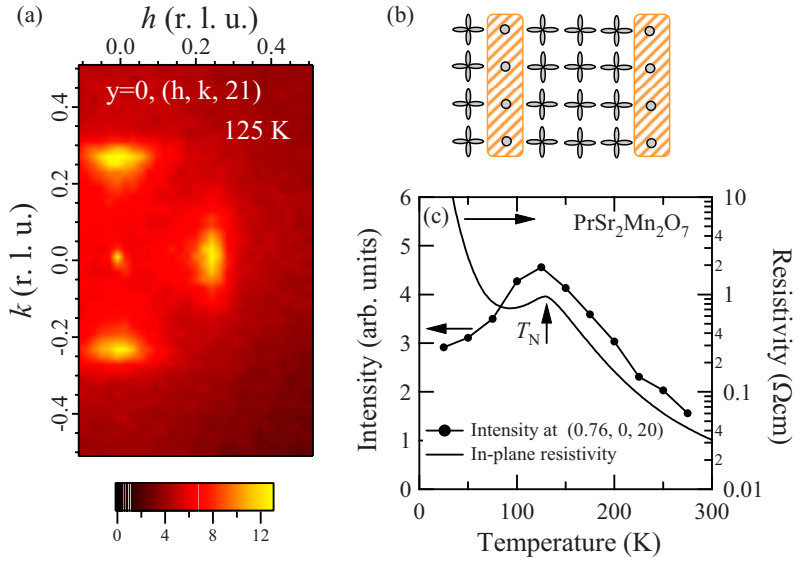

FIG. 6. (Color online) (a) Contour map at around (h, k, 21) with $-0.1 \leqslant h \leqslant 0.5$ and $-0.5 \leqslant k \leqslant 0.5$ for $PrSr_2Mn_2O_7$ obtained by SR x-ray measurements at 125 K. (b) Schematic of the charge stripes with $q=0.25$. (c) Temperature dependence of the peak intensity at (0.76, 0, 20) (filled circle) and in-plane component of ρ_{ab} (solid line) for $PrSr_2Mn_2O_7$.

$\boldsymbol{q}=\pm\boldsymbol{a}^*/2$ appear instead, indicating the orbital stripe running along the b axis, as depicted in Fig. 5(d). This phenomenon is also captured by the reversal of bright and dark contrasts in the DFIs. Figures 5(e) and 5(f) show the DFIs with the aperture position fixed. The bright and dark regions correspond to structural twins of the averaged structure, in which the respective orbital stripe directions are different by 90°. Bright and dark contrasts are observed to be exchanged at around T_{CO2} because the orbital stripe direction is rotated by 90° in each twin domain. It is worth noting in Fig. 4 that the temperature region of the CO1 phase becomes narrower with decreasing y and positions only right below the T_{CO1} for $0.4<y<0.7$, implying some role of the spin correlation developed right below T_{CO1} in stabilizing the CO2 phase. We show in Fig. 6(a) a contour map of the x-ray scattering intensity for $PrSr_2Mn_2O_7$ ($y=0$) in the reciprocal space of (h, k, 21) with $-0.1 \leqslant h \leqslant 0.5$ and $-0.5 \leqslant k \leqslant 0.5$ at $T=125$ K obtained by SR x-ray measurements. Diffuse scattering peaks are observed at the positions of (± 0.24, 0, 21) and (0, ± 0.24, 21), suggesting the existence of a vertical stripe-type CO, as depicted in Fig. 6(b). The coexistence of the diffuse superlattice spot along the a^* and b^* axes is ascribed to the formation of nanoscaled domains with propagation vector along the [100] and [010] directions. The peak intensity first increases as the temperature decreases, then shows the maximum at around T_N [see Fig. 6(c)]. Although the intensity decreases below T_N, it remains down to the lowest temperature.

A similar broad superlattice structure in the "vertical" directions is also reported in other bilayer and perovskite manganites. The modulation wave number here is $q \sim 0.25$, which slightly differs from other nearly half-doped cases [$q \sim 0.3$ for $La_{2-2x}Sr_{1+2x}Mn_2O_7$ ($x=0.4 \sim 0.5$) (Refs. 16 and 17) and $Pr_{0.5}Sr_{0.5}MnO_3$ (Ref. 18)] but rather similar to lower hole-doping cases [$La_{2-2x}Sr_{1+2x}Mn_2O_7$ ($x=0.3 \sim 0.4$) (Ref. 16) and $La_{0.85}Ca_{0.15}MnO_3$ (Ref. 19)]. Such a difference may originate from the difference in the Fermi-surface nesting vector, as first pointed out by the angle-resolved photoemission study on the $La_{2-2x}Sr_{1+2x}Mn_2O_7$ ($x=0.4$).[6]

We did the same measurement on $y=0.2$ and 0.3 compositions (not shown). As increasing y, the intensity of the superlattice reflection is suppressed. Instead, the peak appears at the position of (1/2, 3/2, 20), indicating a structural transition from tetragonal to orthorhombic. Such a structural-transition temperature is plotted as T_S in Fig. 4. Such a "diagonal" lattice deformation as in the orthorhombic form may destabilize the formation of vertical-type charge stripes, while stabilizing the diagonal CO-OO, as manifested by the phase diagram in Fig. 4.

The phase diagram established here bears some analogy to that of half-doped perovskite $Pr_{0.5}(Sr_{1-y}Ca_y)_{0.5}MnO_3$.[13] End materials in both cases have similar ground states; the Sr end shows A-AF with vertical-type short-range CO (Ref. 18) and the Ca end shows CE-AFI with diagonal-type long-range CO-OO. A major difference from the pseudocubic perovskite case is the absence of the FM metallic phase. On the contrary, the half-doped single-layered system never shows long-range A-AF nor FM phase, while the small W and small A-site disorder crystals such as $Pr_{0.5}Ca_{1.5}MnO_4$ raise T_{CO} above room temperature.[20,21] These differences well reflect the differences in the dimensionality and crystal field of each system. The DE kinetic energy gain should less effectively work in the bilayered manganites,[22] relatively stabilizing the x^2-y^2-type OO and A-AF phase as the 2D form of the DE interaction.

In summary, we have investigated the electronic-phase diagram of half-doped bilayered manganite $Pr(Sr_{1-y}Ca_y)_2Mn_2O_7$. For $y \leqslant 0.4$, the A-type AF state with x^2-y^2 orbital order shows up as the ground state while accompanying the short-range vertical charge stripe. For $y>0.4$, the CE-type AF state emerges with the ordered orbital $(3x^2-r^2/3y^2-r^2)$ whose diagonal stripes undergo the 90° rotation with decreasing temperature.

This work was in part supported by Grant-in-Aids for Scientific Research from the MEXT (Nos. 17340104, 15104006, and 16076205), Japan.

[1] Y. Tokura, Rep. Prog. Phys. **69**, 797 (2006).
[2] Y. Moritomo, Y. Tomioka, A. Asamitsu, Y. Tokura, and Y. Matsui, Phys. Rev. B **51**, 3297 (1995).
[3] M. Kubota, H. Fujioka, K. Hirota, K. Ohoyama, Y. Moritomo, H. Yoshizawa, and Y. Endoh, J. Phys. Soc. Jpn. **69**, 1606 (2000).
[4] J. F. Mitchell, C. D. Ling, J. E. Millburn, D. N. Argyriou, A. Berger, and M. Medarde, J. Appl. Phys. **89**, 6618 (2001).
[5] D. S. Dessau, T. Saitoh, C.-H. Park, Z.-X. Shen, P. Villella, N. Hamada, Y. Moritomo, and Y. Tokura, Phys. Rev. Lett. **81**, 192 (1998).
[6] Y.-D. Chuang, A. D. Gromko, D. S. Dessau, T. Kimura, and Y. Tokura, Science **292**, 1509 (2001).
[7] Y. Tokunaga, T. Lottermoser, Y. Lee, R. Kumai, M. Uchida, T. Arima, and Y. Tokura, Nat. Mater. **5**, 937 (2006).
[8] L. M. Rodriguez-Martinez and J. P. Attfield, Phys. Rev. B **54**, R15622 (1996).
[9] P. D. Battle, J. E. Millburn, M. J. Rosseinsky, L. E. Spring, J. F. Vente, and P. G. Radaelli, Chem. Mater. **9**, 3136 (1997).
[10] P. D. Battle, M. A. Green, N. S. Laskey, J. E. Millburn, P. G. Radaelli, M. J. Rosseinsky, S. P. Sullivan, and J. F. Vente, Phys. Rev. B **54**, 15967 (1996).
[11] Y. Moritomo, A. Nakamura, K. Ohoyama, M. Ohashi, and K. Hirota, J. Phys. Soc. Jpn. **68**, 631 (1999).
[12] H. Kuwahara, T. Okuda, Y. Tomioka, A. Asamitsu, and Y. Tokura, Phys. Rev. Lett. **82**, 4316 (1999).
[13] Y. Tomioka and Y. Tokura, Phys. Rev. B **66**, 104416 (2002).
[14] D. Akahoshi, M. Uchida, Y. Tomioka, T. Arima, Y. Matsui, and Y. Tokura, Phys. Rev. Lett. **90**, 177203 (2003).
[15] Y. Tomioka and Y. Tokura, Phys. Rev. B **70**, 014432 (2004).
[16] M. Kubota, Y. Oohara, H. Yoshizawa, H. Fujioka, K. Shimizu, K. Hirota, Y. Moritomo, and Y. Endoh, J. Phys. Soc. Jpn. **69**, 1986 (2000).
[17] B. J. Campbell, R. Osborn, D. N. Argyriou, L. Vasiliu-Doloc, J. F. Mitchell, S. K. Sinha, U. Ruett, C. D. Ling, Z. Islam, and J. W. Lynn, Phys. Rev. B **65**, 014427 (2001).
[18] R. Kajimoto, H. Yoshizawa, Y. Tomioka, and Y. Tokura, Phys. Rev. B **66**, 180402(R) (2002).
[19] P. Dai, J. A. Fernandez-Baca, N. Wakabayashi, E. W. Plummer, Y. Tomioka, and Y. Tokura, Phys. Rev. Lett. **85**, 2553 (2000).
[20] M. Ibarra, R. Retoux, M. Hervieu, C. Autret, A. Maignan, C. Martin, and B. Raveau, J. Solid State Chem. **170**, 361 (2003).
[21] R. Mathieu, M. Uchida, Y. Kaneko, J. P. He, X. Z. Yu, R. Kumai, T. Arima, Y. Tomioka, A. Asamitsu, Y. Matsui, and Y. Tokura, Phys. Rev. B **74**, 020404(R) (2006).
[22] R. Maezono, S. Ishihara, and N. Nagaosa, Phys. Rev. B **57**, R13993 (1998).